

Influence of Electron Blocking Layer on Properties of InGaN-Based Laser Diodes Grown by Plasma-Assisted Molecular Beam Epitaxy

M. HAJDEL^{a,*}, G. MUZIOL^a, K. NOWAKOWSKI-SZKUDLAREK^a, M. SIEKACZ^a,

A. FEDUNIEWICZ-ŻMUDA^a, P. WOLNY^a AND C. SKIERBISZEWSKI^{a,b}

^aInstitute of High Pressure Physics, Polish Academy of Sciences,

Sokołowska 29/37, PL-01142 Warsaw, Poland

^bTopGaN Ltd, Sokołowska 29/37, PL-01142 Warsaw, Poland

We investigate influence of Mg doping concentration and the thickness of electron blocking layer on properties of InGaN-based laser diodes grown by plasma-assisted molecular beam epitaxy. Using simple measurements of light-current characteristics and simulations, two main conclusions are drawn. First one — the Mg dopant is responsible for optical losses, as in the case of the laser diodes grown by metalorganic vapor phase epitaxy. Second one — the low Mg doping causes electrons to overflow through electron blocking layer. Additionally, tunneling is proposed as an escape mechanism of carriers from active region for thin electron blocking layer.

DOI: [10.12693/APhysPolA.136.593](https://doi.org/10.12693/APhysPolA.136.593)

PACS/topics: InGaN lasers, optical losses, Mg doping, EBL thickness, PAMBE

1. Introduction

InGaN based laser diodes (LDs) are attracting a lot of attention as efficient light emitters for displays, data storage, and general lighting [1]. The crucial parameter that limits the output power of III-nitride LDs are the internal optical losses (α_i). First InGaN LDs suffered from high $\alpha_i \approx 40 \text{ cm}^{-1}$ [2, 3] and because of that the maximum values of optical power in the order of 100 mW. Nowadays, state of the art LDs have $\alpha_i = 1 \text{ cm}^{-1}$ and the maximum optical power is 7.2 W [4]. It was shown that, in the case of InGaN-based LDs, the high α_i originates from light absorption in the Mg-doped layers [5–11].

Calculation of Kioupakis et al. have shown that absorption cross-section of Si and Mg do not differ much. However, the higher concentrations of Mg dopant used in III-nitride LDs might have the dominant impact on large α_i values [9, 10]. Due to high activation energy of Mg atoms, the concentration of Mg has to be high enough to ensure sufficient electrical conductivity of *p*-type layers. In case of III-nitride LDs the most highly Mg-doped layer is the electron blocking layer (EBL). It is introduced after the active region to block the overflow of electrons that comes from the difference in mobility of electrons and holes in GaN [12, 13]. Without this Mg-doped layer the injection efficiency (η_i) of carriers into the active region would be low, and the overall efficiency of the LD will drop. It was shown that in order to reduce the total α_i one can introduce an undoped layer placed between

active region and *p*-type doped layers [8, 11]. It decreases the optical confinement factor of Mg-doped layers (Γ_{Mg}) and thus decreases the α_i leading to an improvement in threshold current density (j_{th}) and slope efficiency (SE). However, after a certain thickness of the undoped layer is reached the η_i starts to drop leading to an interplay between α_i and η_i . This makes the designing of *p*-type layers a crucial issue for developing high performance LD.

Majority of the papers have reported the LDs grown by the metalorganic vapor phase epitaxy (MOVPE) technique. Recent advancement in the plasma assisted molecular beam epitaxy (PAMBE) technology in the growth of III-nitride LDs, especially the demonstration of LDs with the lifetime of 100 000 hours [14], allows us to answer the question whether the Mg dopant also causes optical losses in PAMBE-grown LDs. Maybe there are additional sources of absorption present only in MOVPE-grown or in PAMBE-grown LDs. Answer to these questions should verify whatever the current understanding of sources of absorption in high power LDs is correct.

In this paper we experimentally investigate the role of Mg-doping level and thickness of EBL on InGaN-based LD parameters such as j_{th} and SE. Based on experimental data and simulations, a model describing the impact of Mg on α_i and η_i is also proposed.

2. Experimental

The LDs were grown in metal-rich conditions by PAMBE, using a VG V90 reactor, on commercially available LUMILOG GaN substrates with threading dislocation densities of the order of $(1-5) \times 10^7 \text{ cm}^{-2}$. LD structure is presented in Fig. 1a. It consists of 700 nm $\text{Al}_{0.07}\text{Ga}_{0.93}\text{N}:\text{Si}$ bottom cladding and 100 nm GaN:Si layer with Si concentration of $2 \times 10^{18} \text{ cm}^{-3}$. Bottom and

*corresponding author; e-mail: hajdel@unipress.waw.pl

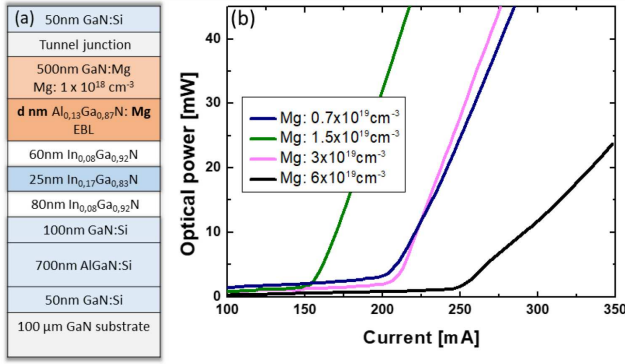


Fig. 1. (a) Structure of studied LDs. The doping and thickness of EBL are varied. (b) Exemplary L-I characteristics of measured LDs.

upper waveguides are undoped $\text{In}_{0.08}\text{Ga}_{0.92}\text{N}$ layers with thickness of 80 nm and 60 nm, respectively. The active region is a 25 nm thick $\text{In}_{0.17}\text{Ga}_{0.83}\text{N}$ quantum well [15]. At the end of the InGaN waveguide the EBL consisting of $\text{Al}_{0.13}\text{Ga}_{0.85}\text{N}:\text{Mg}$ is placed. Upper cladding is a 500 nm *p*-type GaN with Mg doping concentration of $1 \times 10^{18} \text{ cm}^{-3}$. This is followed by a TJ [16] capped with GaN:Si contact layer. Two sets of samples were realized with different designs of EBL. In the first set, the Mg doping levels were changed $(0.7, 1.5, 3, 6) \times 10^{19} \text{ cm}^{-3}$ for a 20 nm thick EBL. In the second set, the doping level was constant at $1.5 \times 10^{19} \text{ cm}^{-3}$ and the thickness was changed, i.e., (5, 10, 20) nm. More details on growth and processing of the devices can be found in [17].

To study the influence of EBL design on properties of LDs the light-current (*L-I*) characteristics of grown samples were measured using an integrating sphere. To avoid the heating effects measurements were done under pulse operation with pulse length of 200 ns. Exemplary *L-I* curves are shown in Fig. 1b. To accurately determine the influence of EBL design in EBL tens of LDs for each sample were measured and j_{th} and SE values were estimated and then averaged. To obtain insight into the physical processes taking place in the LD the band diagrams and η_i of grown devices were simulated using SiLENSe software [18]. Optical mode distribution and confinement factors were calculated using a 1D model [19].

3. Results and discussion

3.1. Mg doping concentration in EBL

Averaged values of j_{th} and SE of LDs with different Mg doping of EBL are presented in Fig. 2a and b, respectively. The error bars depict the standard deviation among the measured devices. For the highest Mg doping the j_{th} and SE are equal to 4.62 kA cm^{-2} and 0.359 W/A , respectively. When the Mg doping is lowered, both j_{th} and SE show an improvement. To understand how Mg influences the internal properties of LDs the following model has been created. The j_{th} and SE are related to

the internal properties by

$$j_{th} = \frac{\alpha_i + \alpha_m}{\Gamma \eta_i \left(\frac{dg}{dj} \right)} + j_{trans}, \quad (3.1)$$

$$SE = \eta_i \left(\frac{\alpha_m}{\alpha_i + \alpha_m} \right) \frac{hv}{q}, \quad (3.2)$$

where α_m are mirror losses, Γ is the confinement factor of active region, g is the material gain, j_{trans} is the transparency current, v is the frequency of emitted light from device, q is the elementary charge, and h is the Planck constant.

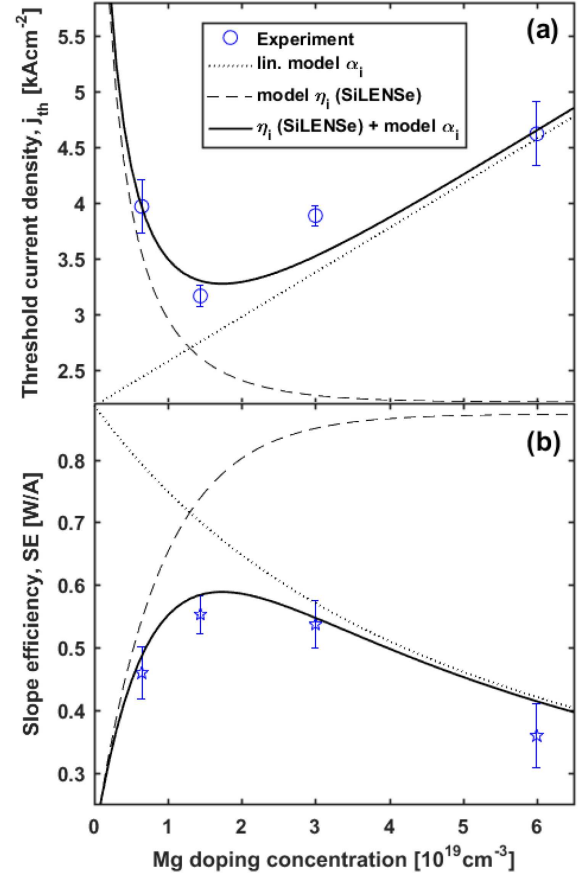


Fig. 2. Dependence of: (a) threshold current density and (b) slope efficiency on Mg doping level in EBL.

To model the impact of Mg doping on optical losses the optical confinement with EBL (Γ_{EBL}) has been calculated. Figure 3 presents the optical mode distribution with the shaded area representing the part of the optical mode involved in light absorption in EBL. The calculated value of Γ_{EBL} is 4.37%. A linear dependence between the absorption and Mg concentration has been assumed by a relation $\alpha_{Mg} = 112 \text{ cm}^{-2} \times \text{Mg concentration}$ (in units of 10^{19} cm^{-3}). Additionally, residual optical losses of $\alpha_0 = 9.5 \text{ cm}^{-1}$ are fitted. The calculated dependence is presented in Fig. 2 as a dotted line. As can be seen, the change of j_{th} and SE in the regime of high Mg doping ($\text{Mg} > 2 \times 10^{19} \text{ cm}^{-3}$) can be explained solely by

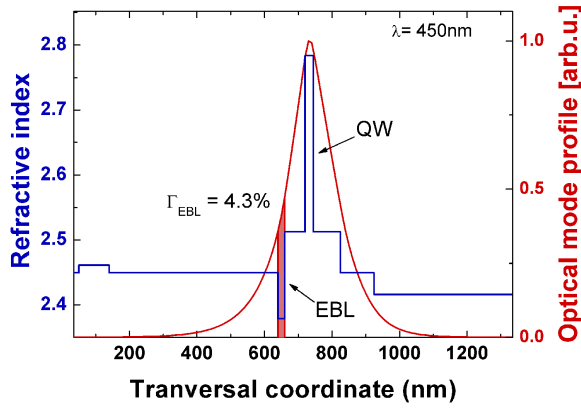


Fig. 3. Refractive index profile and optical mode distribution of studied LDs. Shaded section correspond to the 20nm EBL.

the change in the optical losses due to absorption on Mg. However, for lower Mg concentrations a growing discrepancy between this model and the experimental data is observed.

To understand this behavior we have used the SiLENSE 5.4 package [18] equipped with a one dimensional drift diffusion model. Figure 4 presents the calculated conduction band profile of the LDs with Mg doping of 0.7×10^{19} and $6.0 \times 10^{19} \text{ cm}^{-3}$. Only the vicinity of the QW and EBL is shown. As can be seen the change of the doping in EBL strongly changes the energetic barrier (E_B) in the conduction band which is used to prevent the electron overflow to the p -type region. The value of E_B decreases from 204 to 105 meV when the Mg doping is changed from 6.0×10^{19} to $0.7 \times 10^{19} \text{ cm}^{-3}$. Such a change affects the injection efficiency. Figure 5 presents the calculated dependence of η_i on current density for several doping levels and thicknesses. For low current density the η_i is independent of the EBL design and is equal to 1, which means that all electrons recombine in the QW region. As the current density is increased, a drop in η_i is observed. This results in a decrease of η_i for low Mg doping as it is shown in the inset in Fig. 5 for a fixed current density of 3 kAcm^{-2} . Taking into account the change of η_i with Mg and assuming a constant α_i the j_{th} and SE can be well modeled in the low Mg doping regime as shown by dashed line in Fig. 2. A model combining the change of both η_i and α_i with Mg is constructed and plotted as a solid line in Fig. 2. This model is in good agreement with the experimental data indicating that both η_i and α_i are affected when the Mg doping level in the EBL is changed. It is important to note that in the model the same fitting parameters are used to describe both the effects on j_{th} and SE.

Based on the proposed model an optimal value of doping in the EBL can be predicted. For a considered structure it is equal to $1.8 \times 10^{19} \text{ cm}^{-3}$. It is worth mentioning that for different structure designs this value can vary, especially if the EBL and/or InGaN waveguide composition are changed, affecting η_i [20].

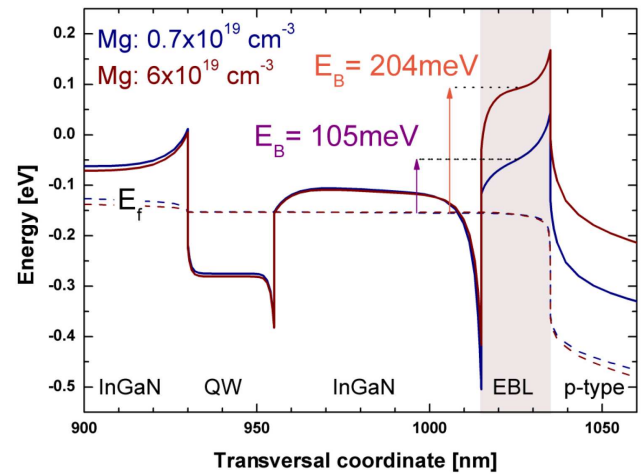


Fig. 4. Calculated conduction band of the LDs with the highest and the lowest Mg doping concentration.

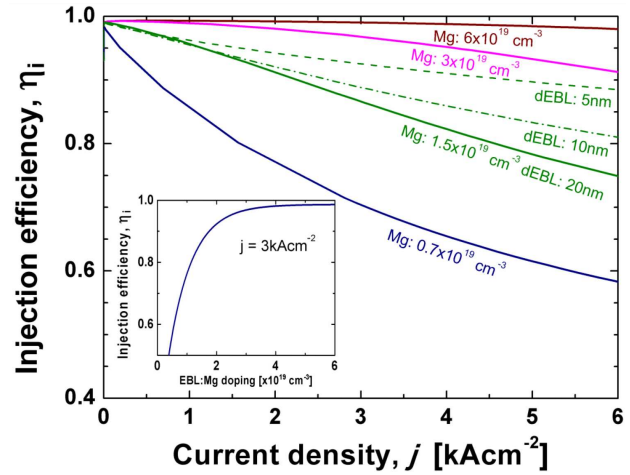


Fig. 5. Simulated dependence of injection efficiency on current density for different Mg doping level for 20 nm thick EBL (and for different thicknesses for a constant doping of $1.5 \times 10^{19} \text{ cm}^{-3}$ - dashed and dash-dot lines).

3.2. EBL thickness

In the second set of samples the EBL thickness is changed. This should affect the optical losses. The reduction of EBL thickness reduces Γ_{EBL} from 4.37% to 1.28% and consequently the α_i from 16.8 cm^{-1} to 11.5 cm^{-1} for 20 nm and 5 nm, respectively. The measured j_{th} and SE are presented in Fig. 6. The decrease of the EBL thickness caused a significant increase of j_{th} and a decrease of SE. To understand the unexpected change in j_{th} and SE once again the band profiles and injection efficiency were calculated. In Fig. 7 one can see the conduction band profile. The height of the energetic barrier remains unchanged, however, its width decreases. The calculated current density η_i is presented in Fig. 5. Its slight increase can be seen when the EBL thickness is reduced.

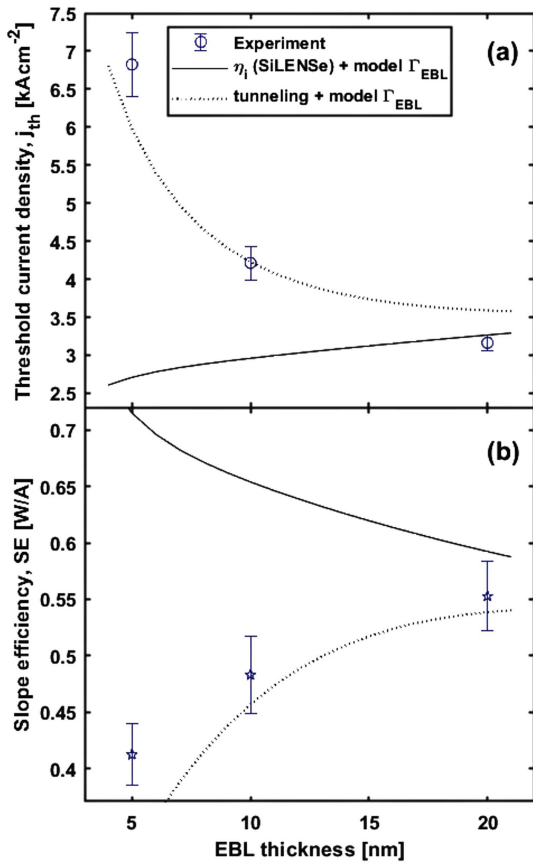


Fig. 6. Dependence of: (a) threshold current density and (b) slope efficiency on EBL thickness.

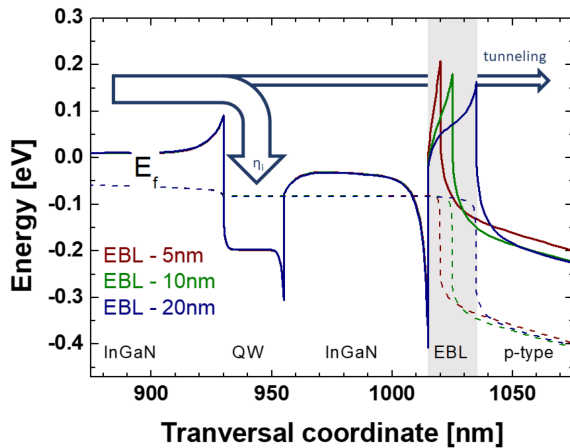


Fig. 7. Calculated conduction band of the LDs with the EBL thickness of 5, 10 and 20 nm. Arrows indicate the electron flow paths.

The model describing the calculated change of α_i and η_i with Mg doping level is presented as a solid line in Fig. 6. The model, based on drift diffusion theory, predicts a decrease of j_{th} and an increase of SE for low EBL thicknesses. Surprisingly, the experimentally measured values show an opposite trend to the presented model.

To correctly describe the experiment we propose an additional effect: tunneling of electrons through EBL. If the EBL thickness is insufficient, a part of the electron current might tunnel even though the height of the energetic barrier remains constant (shown by an arrow in Fig. 7). A simple model of reduction of η_i by tunneling is described by

$$\eta'_i = \eta_i(1 - T), \quad (3.3)$$

where T is tunneling probability. In general, it could be described also as an exponential function dependent on the barrier thickness d , i.e.,:

$$T = e^{-k d}. \quad (3.4)$$

The model including the change of η'_i and α_i with EBL thickness is presented in Fig. 6, as a dotted line. The fitting parameter is $k = 0.16$. This concept qualitatively explains the drop of SE and the increase of j_{th} observed for low EBL thickness, indicating also that the drift-diffusion model fails at thicknesses below 20 nm. Further work has to be done to verify whether the 20 nm EBL is sufficient to prevent tunneling.

4. Summary

The influence of Mg doping and thickness of electron blocking layer on threshold current density and slope efficiency of InGaN LDs was studied. It was found that Mg is responsible for optical losses in LDs grown by PAMBE. Decrease of Mg doping in EBL improves the performance of studied LDs. However, if the Mg doping is too low, a decrease of injection efficiency is observed. Additionally, a strong overflow by means of tunneling of electrons through EBL was proposed to describe the experimentally observed change of j_{th} and SE in samples with thin EBL. Estimating the optimum Mg doping level and EBL thickness brings us one step further to the development of reliable high power InGaN laser diodes.

Acknowledgments

This work has been partially supported by TEAM-TECH POIR.04.04.00-00-210C/16-00 project of the Foundation for Polish Science co-financed by the European Union under the European Regional Development Fund the National Centre for Research and Development grants LIDER/29/0185/L-7/15/NCBR/2016 and LIDER/35/0127/L-9/17/NCBR/2018.

References

- [1] J.J. Wierer, J.Y. Tsao, D.S. Sizov, *Laser Photon Rev.* **7**, 963 (2013).
- [2] U.T. Schwarz, E. Sturm, W. Wegscheider, *Appl. Phys. Lett.* **83**, 4095 (2003).
- [3] M. Kuramoto, C. Sasaoka, N. Futagawa, M. Nido, A.A. Yamaguchi, *Phys. Status Solidi A* **192**, 329 (2002).

- [4] M. Kawaguchi, O. Imafuji, S. Nozaki, H. Hagino, S. Takigawa, T. Katayama, T. Tanaka, *Proc. SPIE* **9748**, 974818 (2016).
- [5] M. Martens, C. Kuhn, T. Simoneit, S. Hagedorn, A. Knauer, T. Wernicke, M. Weyers, M. Kneissl, *Appl. Phys. Lett.* **110**, 081103 (2017).
- [6] Ohad Westreich, Moti Katz, Gil Atar, Yossi Paltiel, Noam Sicon, *Appl. Phys. Lett.* **111**, 022103 (2017).
- [7] D. Sizov, R. Bhat, C. Zah, *J. Appl. Phys.* **113**, 203108 (2013).
- [8] S. Uchida, M. Takeya, S. Ikeda, T. Mizuno, T. Fujimoto, O. Matsumoto, S. Goto, T. Tojyo, M. Ikeda, *IEEE J. Sel. Top. Quant. Electron.* **9**, 1252 (2003).
- [9] E. Kioupakis, P. Rinke, C.G.V. de Walle, *Appl. Phys. Expr.* **3**, 082101 (2010).
- [10] E. Kioupakis, P. Rinke, A. Schleife, F. Bechstedt, C.G. Van de Walle, *Phys. Rev. B* **81**, 241201(R) (2010).
- [11] G. Muziol, H. Turski, M. Siekacz, P. Wolny, S. Grzanka, E. Grzanka, P. Perlin, C. Skierbiszewski, *Appl. Phys. Expr.* **8**, 032103 (2015).
- [12] D.K. Gaskill, L.B. Rowland, K. Doverspike, in: *Properties of Group III Nitrides*, Ed. J.H. Edgar, EMIS Datareviews Series, INSPEC 1995, p. 101.
- [13] W. Götz, N.M. Johnson, C. Chen, H. Liu, C. Kuo, W. Imler, *Appl. Phys. Lett.* **68**, 3144 (1996).
- [14] G. Muziol, M. Siekacz, K. Nowakowski-Szkudlarek, M. Hajdel, J. Smalc-Koziorowska, A. Feduniewicz-Żmuda and E. Grzanka, P. Wolny, H. Turski, P. Wiśniewski, P. Perlin, C. Skierbiszewski, *Mater. Sci. Semicond. Proc.* **91**, 387 (2019).
- [15] G. Muziol, M. Hajdel, M. Siekacz, K. Szkudlarek, S. Stanczyk, H. Turski, C. Skierbiszewski, *Appl. Phys. Expr.* **12**, 072003 (2019).
- [16] C. Skierbiszewski, G. Muziol, K. Nowakowski-Szkudlarek, H. Turski, M. Siekacz, A. Feduniewicz-Zmuda, A. Nowakowska-Szkudlarek, M. Sawicka, P. Perlin, *Appl. Phys. Expr.* **11**, 034103 (2018).
- [17] C. Skierbiszewski, H. Turski, G. Muziol, M. Siekacz, M. Sawicka, G. Cywiński, Z.R. Wasilewski, S. Porowski, *J. Phys. D Appl. Phys.* **47**, 073001 (2014).
- [18] STR, SiLENSe 5.4 package.
- [19] G. Muziol, H. Turski, M. Siekacz, S. Grzanka, P. Perlin, C. Skierbiszewski, *Appl. Phys. Expr.* **9**, 092103 (2016).
- [20] G. Muziol, H. Turski, M. Siekacz, P. Wolny, J. Borysiuk, S. Grzanka, P. Perlin, C. Skierbiszewski, *Opt. Expr.* **25**, 33113-33121 (2017).